OPTIMIZATION OF EARTH FLIGHT TEST TRAJECTORIES TO QUALIFY PARACHUTES FOR USE ON MARS

Christopher L. Tanner[(1)]

[(1)]*Space Systems Design Laboratory, Daniel Guggenheim School of Aerospace Engineering*
Georgia Institute of Technology, 270 Ferst Drive, Atlanta, GA 30332-0150, United States
Email: christopher.tanner@gatech.edu

ABSTRACT

This paper presents a simulation designed to optimize Earth flight test trajectories of parachute-payload systems. These trajectories attempt to replicate the conditions experienced by a parachute during supersonic descent through the Martian atmosphere. The critical parameters that need to be closely matched in a supersonic flight test are the peak opening load and the parachute load time history, both of which are key parameters to parachute structural qualification. To investigate the associated Earth flight test requirements, descent trajectories and parachute loading profiles are generated for a 4,000 kg payload using a 30 m nominal diameter disk-gap-band parachute deployed at Mach 3 on Mars. Subsequent Earth flight test trajectories are optimized and compared to the reference Mars cases. Both Mars and Earth simulations use two different parachute loading models: an inflation curve and an apparent mass model. Given the same initial conditions, both models generate similar results, but trajectory optimization using each model generates different Earth flight conditions. Finally, a brief investigation into the aerodynamic heating experienced by a supersonic parachute on both Earth and Mars is performed and compared to observed DGB heating profiles.

NOMENCLATURE

Symbols

C_DS	Parachute drag area
$C_{D,0}$	Parachute steady-state drag coefficient
C_x	Inflation curve opening load factor
D_0	Parachute nominal diameter
D_v	Test vehicle diameter
F_p	Parachute load
$F_{p,max}$	Peak opening load at parachute full inflation
$F_{p,avg}$	Average parachute load over a period of time
L	Inflation distance
M	Mach number
$F(\bar{x})$	Optimizer objective function
S_0	Parachute nominal area
S_p	Parachute projected area
S_r	Parachute projected area ratio
V	Velocity
a	Speed of sound
g	Acceleration due to gravity
h	Altitude
h_0	Initial altitude at line stretch
k_0	Apparent mass constant
m_a	Parachute apparent mass
m_p	Parachute canopy mass
m_v	Test vehicle mass
n	Inflation curve exponent
q	Dynamic pressure
t	Time
t_{FI}	Time at full inflation
t_{fill}	Parachute inflation time
t_{LS}	Time at parachute line stretch
$t_{M=1.5}$	Time, measured from full inflation, until the vehicle decelerates to Mach 1.5
t_{SI}	Time at start of inflation, assumed to occur at parachute line stretch
$\bar{x}$	Vector of design variables
α	Inflation distance constant
β	Ballistic coefficient
γ	Flight path angle OR ratio of specific heats
γ_0	Flight path angle at start of inflation of Earth flight test
γ_{Mars}	Flight path angle at start of inflation of reference Mars trajectory
ρ	Fluid density
$\Delta F_{p,avg}$	Percent difference in average parachute load between Earth and Mars trajectories
$\Delta F_{p,max}$	Percent difference in peak opening load between Earth and Mars trajectories
$\Delta t_{M=1.5}$	Percent difference in time from full inflation to Mach 1.5 between Earth and Mars trajectories

Acronyms

BLDT	Balloon-Launched Decelerator Test
DGB	Disk-gap-band
DOF	Degrees of freedom
EoMs	Equations of motion
IC	Initial condition
NASA	National Aeronautics and Space Administration

1. MODELS

1.1. Equations of Motion

The following assumptions are made in deriving the EoMs:

1) A flat, non-rotating planet with no winds.
2) The parachute is rigidly connected to the payload.
3) Only drag forces are considered.
4) There are only two degrees of freedom, with motion constrained to a single plane.

The EoMs that are used in the trajectory simulation are:

$$\begin{aligned}\frac{dV}{dt} &= -\frac{\rho V^2}{2\beta} - g\sin\gamma \\ \frac{d\gamma}{dt} &= -\frac{g\cos\gamma}{V} \\ \frac{dh}{dt} &= V\sin\gamma\end{aligned} \tag{1}$$

where V is the system's velocity, ρ is atmospheric density at altitude, β is the system's ballistic coefficient (mass divided by drag area), g is the local acceleration due to gravity, γ is the flight path angle (positive above the horizon), and h is altitude.

1.2. Inflation Models

To capture the force* associated with the parachute inflation, two separate parachute inflation models are employed: an inflation curve model and an apparent mass model.

The inflation curve model† is an empirical inflation model that assumes a given drag area growth profile and that the peak load is related to the steady-state force of the parachute by an assumed opening load factor (C_x). Parachute force (F_p) represented by the inflation curve model is given in Eq. 2.

$$F_p = \begin{cases} qC_{D,0}S_0C_x\left(\dfrac{t-t_{SI}}{t_{FI}-t_{SI}}\right)^n + m_p g\sin\gamma & t_{SI} \le t \le t_{FI} \\ qC_{D,0}S_0 + m_p g\sin\gamma & t > t_{FI} \end{cases} \tag{2}$$

where q is the dynamic pressure, $C_{D,0}$ is the steady-state parachute drag coefficient, S_0 is the nominal parachute area, t is time, t_{SI} is the time at start of inflation, t_{FI} is the time at full inflation, and n is the inflation curve exponent, which defines the drag area growth profile. The accuracy of this method depends on proper selection of values for C_x and n.

The apparent mass model [1] attempts to improve the physics model of parachute inflation by including effects of the air mass. During the inflation process, the parachute accumulates air mass within and around the canopy – mass referred to as *apparent mass*. This mass becomes part of the parachute-payload system and subsequently yields additional terms in parachute force equation. A revised parachute force equation that accounts for apparent mass is shown in Eq. 3.

$$F_p = qC_DS + \frac{d}{dt}\left[\left(m_a + m_p\right)V\right] + m_p g\sin\gamma \tag{3}$$

where C_DS is the parachute drag area, m_a is the apparent mass, and m_p is the parachute canopy mass. The C_DS term is the change in quasi-steady-state drag area of the parachute during inflation and is assumed to be

$$C_DS = C_{D,0}S_0S_r \tag{4}$$

where S_r is the parachute projected area ratio ($S_r = S_p / S_{p,\max}$) at a given point during the inflation. S_p is the parachute's projected area, which changes with time, and $S_{p,max}$ is the maximum projected area, attained at full inflation. The apparent mass is modeled as

$$m_a = k_0\rho\left(\frac{\pi D_0^3}{12}\right)S_r^{3/2} \tag{5}$$

where k_0 is a non-dimensional, empirical constant and the $\pi D_0^3/12$ term is the volume of a hemisphere of diameter D_0. Differentiating Eq. 5 with respect to time and assuming that $d\rho/dt$ is small over the time period of interest, results in

$$\frac{dm_a}{dt} = \frac{3}{2}k_0\rho\left(\frac{\pi D_0}{12}\right)S_2^{1/2}\frac{dS_r}{dt} \tag{6}$$

To obtain a parachute force time history, a trajectory providing q, ρ, V, and $C_{D,0}$ time histories is required. The difficulty in implementing this apparent mass model lies in the determination of an appropriate time dependence for S_r and dS_r/dt as well as a value for k_0,.

1.3. Inflation Time

In order to use either of the parachute force models described above, the inflation time of the parachute must be known. Greene[2] presents a method to predict a parachute's opening *distance* as a function of the parachute's diameter and Mach number at the start of inflation. Greene's inflation distance (L) model is given by

---

* *Force* is used to denote aerodynamic forces only; *load* is used to denote aerodynamic and non-aerodynamic (i.e. mortar recoil, snatch) forces. Since non-aerodynamic forces are not calculated in this study, aerodynamic forces are used as a surrogate for parachute load.

† Obtained from unpublished work by Dr. Juan R. Cruz.

$$L = \frac{(\gamma+1)M_\infty^2}{(\gamma-1)M_\infty^2+2}\left(1+\frac{\gamma-1}{2}M_D^2\right)^{1/\gamma-1}\alpha D_0$$
$$M_D^2 = \frac{(\gamma-1)M_\infty^2+2}{2\gamma M_\infty^2-\gamma+1} \quad (7)$$

where γ is the ratio of specific heats of the fluid (not to be confused with flight path angle), M_∞ is the freestream Mach number, and α is an empirical constant dependent on the canopy geometry. Knowledge of a parachute's opening distance is useful in the case of an infinite mass inflation (i.e. constant velocity) as inflation time can be directly estimated from the deployment velocity. This type of inflation is indicative of supersonic parachutes in thin atmospheres, such as that experienced at Mars or in a high-altitude flight test on Earth.

Greene assumed in his analysis that a normal shock exists in front of the parachute canopy during inflation, the velocity of the air inside the canopy is essentially zero, and that the gas behaves as a perfect gas. The assumptions underlying Greene's model have been subject to scrutiny and criticism, however. Wolf [3] argued that the assumption of a normal shock in front of the parachute during inflation is invalid. In Wolf's analysis, the relative mass of the parachute canopy to the air mass contained within the fully-inflated canopy (referred to as the parachute mass ratio) is a key parameter that is absent from Greene's model. In other words, a parachute canopy that has more relative inertia than the fluid contained within the canopy (such as the case in a low-density atmosphere) will experience a slower inflation time. This makes sense physically, as it will take longer for the relatively low inertia air mass to impart movement on the relatively high inertia canopy fabric.

However, it should be noted that both Greene and Wolf used essentially the same data to calibrate their fundamentally different models. In spite of the differences, both models are capable of reproducing the available data to the same degree of accuracy. This is due to the fact that Mach number and parachute mass ratio effects cannot be separated using the available data. Since both Wolf and Greene appear to be able to predict inflation time with the same accuracy, and Greene's method is substantially easier to implement, Greene's method is employed in this analysis.

2. MODEL CALIBRATION AND VALIDATION

To determine representative values for each of the model parameters described above, both parachute force models were calibrated against data from the Balloon Launched Decelerator Test (BLDT) program vehicle AV-4 flight test [4]. The 2-DOF simulation was subsequently validated against the available AV-4 trajectory data using the calibrated parachute force models. The conditions at AV-4 mortar fire, summarized in Table 1, were used as the initial conditions (ICs) the simulation validation.

Table 1. AV-4 flight test parameters.

Test vehicle mass	m_v	860.5 kg
Test vehicle diameter	D_v	3.51 m
Parachute mass	m_p	37.6 kg
Parachute nominal diameter	D_0	16 m
Initial state (at mortar fire)	h_0	44,862 m
	V_0	698.1 m/s
	γ_0	12.3°
Time (from mortar fire)	t_{SI}	0.985 s
	t_{FI}	1.545 s
Parachute Inflation Time	t_{fill}	0.56 s

2.1. Calibration of Key Parameters

The empirical constants in both the inflation curve and apparent mass models were tuned using AV-4 inflation data. Fig. 1 shows very good agreement between the simulated and observed parachute area ratio growth profile of AV-4. The only difference exists at peak inflation where AV-4 undergoes a slight over-inflation which is not accounted for in the present models.

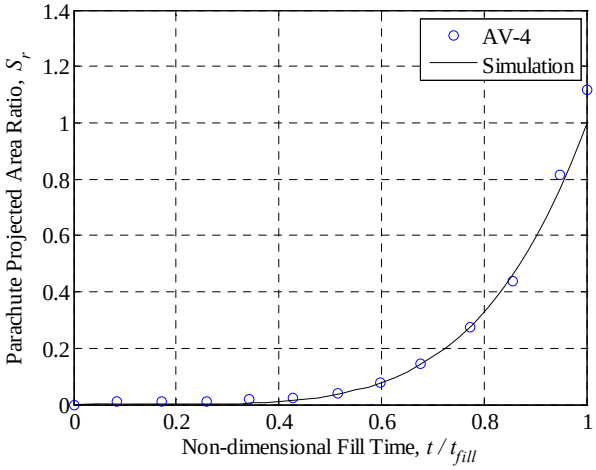

Fig. 1. Parachute projected area ratio profile for inflation curve and apparent mass models.

Because of the excellent fit between the inflation curve modeled in Fig. 1 and AV-4, the same relationship was used to model S_r in the apparent mass model. Since S_r is specified as an analytic expression, its derivative is easily found to provide an analytic relationship for dS_r/dt. The relationships for both S_r and dS_r/dt are given below in Eq. 8.

$$S_r = \left(\frac{t - t_{SI}}{t_{FI} - t_{SI}} \right)^5$$
$$\frac{dS_r}{dt} = \frac{5(t - t_{SI})^4}{(t_{FI} - t_{SI})^5} \quad (8)$$

The empirical coefficient α used in Greene's inflation distance model was calibrated to match the actual AV-4 inflation time. A summary of the observed AV-4 data and the calibrated empirical terms for each model is given below in Table 2.

Table 2. Summary of model calibration values.

AV-4 flight data	$F_{p,max}$	72,043 N
	t_{fill}	0.560 s
Inflation curve model parameters	C_x	1.529
	n	5
	$F_{p,max}$	72,064 N
Apparent mass model parameters	k_0	1.426
	$F_{p,max}$	72,045 N
	S_r	Eq. 8
	dS_r/dt	Eq. 8
Opening distance parameters	α	7.39
	t_{fill}	0.560 s

2.2. Trajectory Validation

Using the ICs prescribed in Table 1, a trajectory simulation was conducted and compared to AV-4 flight data, shown in Fig. 2a – 2c.

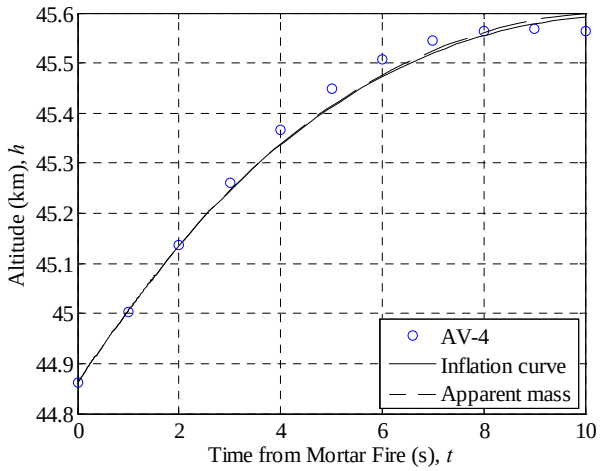

(a) Time vs. Altitude

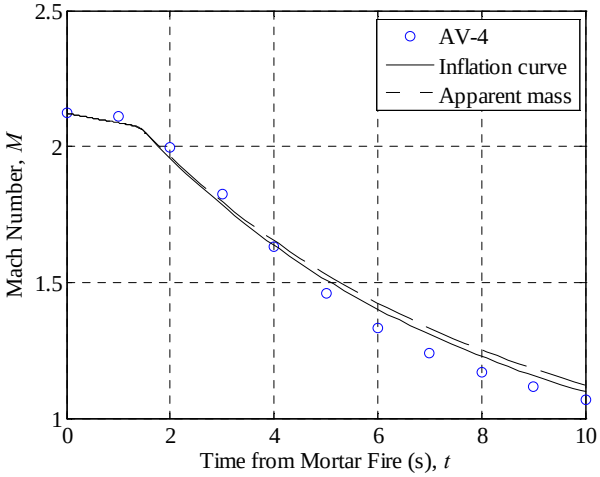

(b) Time vs. Mach Number

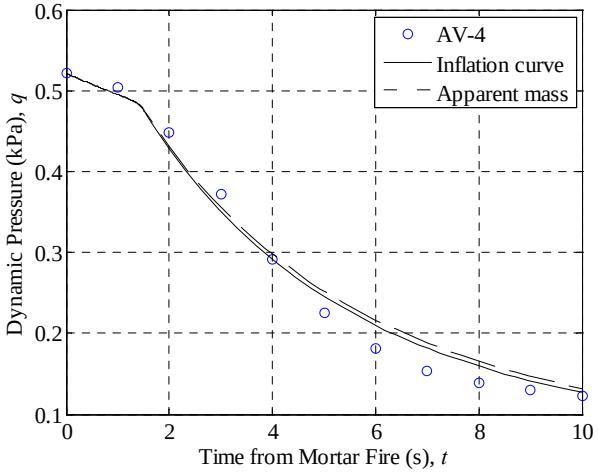

(c) Time vs. Dynamic Pressure

Fig. 2. Trajectory comparison of simulation vs. AV-4 flight data.

In general, Fig. 2 shows good agreement between the AV-4 flight test data and the simulation until about 10 sec. This deviation after 10 sec was also observed by Talay [5], who cited winds during the test flight (which were not modeled) as the primary culprit.

3. EARTH FLIGHT TEST OPTIMIZATION

The goal of this analysis is to develop optimized flight test trajectories on Earth that can accurately reproduce the parachute peak load and load time history experienced by the parachute during inflation on Mars. The optimization problem to generate these trajectories is posed as:

Minimize: $$F(\bar{x}) = \int_{t_{FI}}^{t_{M=1.5}} \left(F_p\big|_{Earth} - F_p\big|_{Mars} \right)^2 dt$$

Subject to: $$F_{p,max}\big|_{Earth} = F_{p,max}\big|_{Mars}$$
$$abs\left(t_{M=1.5}\big|_{Earth} - t_{M=1.5}\big|_{Mars} \right) \le tol$$

Design Variables:

$$\bar{x} = \begin{Bmatrix} m_v \\ h_0 \\ \gamma_0 \end{Bmatrix}$$

3.1. Design Variables

In an actual Earth flight test, there are realistically three parameters that can be controlled in order achieve the desired flight conditions: the mass of the test vehicle (m_v), the altitude at which the parachute begins inflation (h_0), and the flight path angle at the start of parachute inflation (γ_0). These three parameters represent the design variables in the optimization posed above.

3.2. Constraints

The two constraints of the optimization problem represent the two most important parameters to match in the flight test of a parachute. The peak load ($F_{p,max}$) is the greatest force which the parachute must withstand, which is important for parachute structural qualification. Thus, the peak load at Earth $\left(F_{p,\max}\big|_{Earth}\right)$ must be equal to the peak load experienced at Mars $\left(F_{p,\max}\big|_{Mars}\right)$. The duration between full inflation and the point at which the system decelerates to Mach 1.5 ($t_{M=1.5}$) is also important. Above Mach 1.5, a DGB canopy typically exhibits rapid opening and collapsing oscillations, with each oscillation subjecting the parachute large amplitude cyclic loads. Around Mach 1.5, the parachute achieves a stable canopy shape, ending the cyclic loads. A tolerance factor (*tol*) of ±10% of the reference $t_{M=1.5}$ is used because exact agreement is not possible (see Section 5.4) and a 10% agreement in an actual flight test would be sufficient.

3.3. Objective Function

Matching the time to Mach 1.5 does not guarantee that the loads experienced during this time will be similar. Thus, the objective function attempts to minimize the sum square error in parachute load between the Earth and Mars trajectories to *most closely* reproduce the force time history between full inflation and Mach 1.5.

4. REFERENCE MARS TRAJECTORIES

To investigate the potential requirements for future parachute qualification, a large payload of 4000 kg was assumed to enter into the Mars atmosphere and deploy a 30 m nominal diameter DGB parachute at Mach 3. The trajectories were started at parachute line stretch (i.e. Mach 3) and considered four flight path angles, γ_{Mars} = 0°, -15°, -30°, and -45°, with a deployment altitude such that allows the vehicle to decelerate to Mach 0.8 at 5,000 m altitude. The rationale behind achieving Mach 0.8 at 5,000 m altitude is based on the work by Braun and Manning [6]. By utilizing a supersonic parachute at Mach 3 to decelerate the vehicle to Mach 0.8 at 5,000 m altitude, there will be ample timeline to complete the descent and landing sequence. Fig. 3 presents the descent trajectory and load profile for the γ_{Mars} = -30° case.

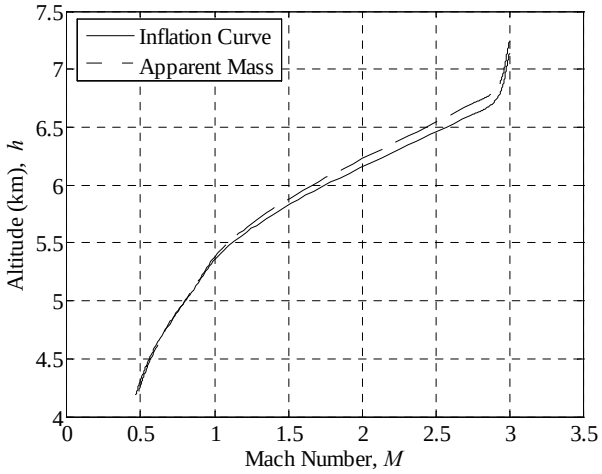

(a) Mach Number vs. Altitude

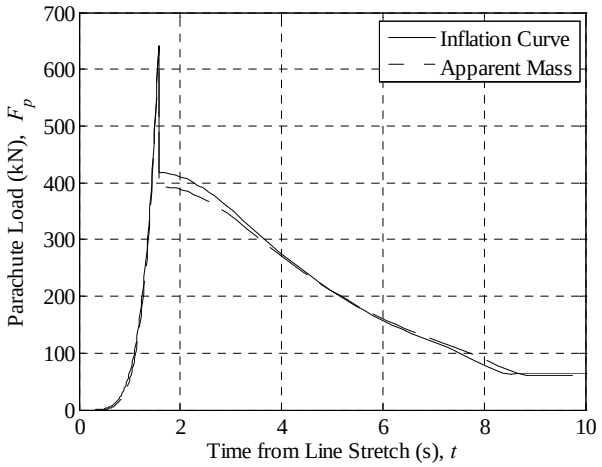

(b) Time from Line Stretch vs. Parachute Load

Fig. 3. Mars trajectory and parachute load time history for γ_{Mars} = -30°.

Table 3 lists the peak load experienced during each case and the time from peak load to Mach 1.5. The longer $t_{M=1.5}$ time is due to the fact that the apparent mass trajectories are initiated at a higher altitude than the inflation curve trajectories (to achieve the Mach 0.8 at 5,000 m condition), which effectively translates into less density to decelerate the vehicle.

Table 3. Pertinent parameters from Mars trajectory.

	Inflation Curve		Apparent Mass	
γ_{Mars} (deg)	$F_{p,max}$ (kN)	$t_{M=1.5}$ (sec)	$F_{p,max}$ (kN)	$t_{M=1.5}$ (sec)
0^o	729.8	2.79	732.9	2.96
-15^o	682.6	3.01	685.9	3.19
-30^o	639.1	3.22	641.3	3.43
-45^o	598.3	3.43	600.1	3.65

5. RESULTS

5.1. System Reponses

There are three parameters (referred to as system responses) that are of interest from the simulation: $\Delta F_{p,max}$, $\Delta t_{M=1.5}$, and $\Delta F_{p,avg}$. The difference in peak opening load, expressed as a percent difference from the reference Mars value, is represented by $\Delta F_{p,max}$. The difference in time between full inflation and Mach 1.5, expressed as a percent, is represented by $\Delta t_{M=1.5}$. Finally, the difference in the time-averaged parachute load between full inflation and Mach 1.5, expressed as a percent of the reference Mars value, is represented by $\Delta F_{p,avg}$. This average parachute load is used in lieu of the optimization objective function $F(\bar{x})$ as a measure of the "goodness" of the optimization because it is hard to determine the relative magnitude of a "good" sum square error. It is easier to understand and compare the relative magnitudes of the average parachute load, which can be plotted on the same chart as the parachute load profile.

Negative response values indicate that the given response at Mars is larger than that at Earth. For example, a negative $\Delta F_{p,max}$ indicates that the peak opening load experienced during Mars descent is greater than the peak opening load obtained during the Earth flight test. "Good" responses are defined as less than a 10% difference between Earth and Mars.

5.2. Optimization of Earth Flight Test Trajectories to Match the Reference Mars Peak Opening Load

A set of Earth flight test initial conditions (ICs) was optimized for each reference Mars trajectory and each parachute force model. These optimal Earth flight test ICs, which occur at line stretch (defined as the start of parachute inflation), and the subsequent system responses are summarized in Table 4. The resulting parachute load profiles are shown in Fig. 4.

Table 4. Optimized flight test parameters for γ_{Mars} = -30 deg.

	Inflation Curve	Apparent Mass
m_v (kg)	2,908.2	2,424.5
h_0 (km)	39,103	40,234
γ_0 (deg)	1.62	-45.3
$\Delta F_{p,max}$	0.0%	0.0%
$\Delta t_{M=1.5}$	7.63%	-8.76%
$\Delta F_{p,avg}$	0.0%	-0.87%

The results in Table 4 show that the optimal set of initial conditions using the inflation curve model differs substantially from those obtained using the apparent mass model. Do the parachute force models differ greatly in their results or do the constraints force the optimizer to a different solution based on a small difference in the parachute force modeling? Results show that the latter case is true. Two simulations were conducted with the ICs swapped – the inflation curve model was utilized with the ICs obtained from the apparent mass optimization and vice versa. The results of these swapped simulations show that the two force models generate similar results given the same initial conditions. Furthermore, it appears that the ICs optimized using the inflation curve model appear to generate a better match to the reference Mars load profile for both force models.

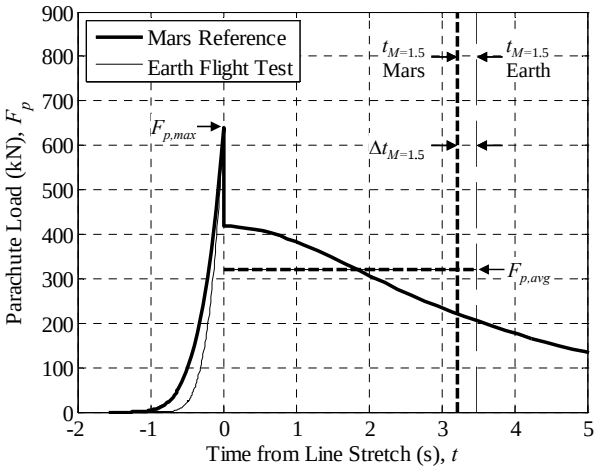

(a) Inflation curve model.

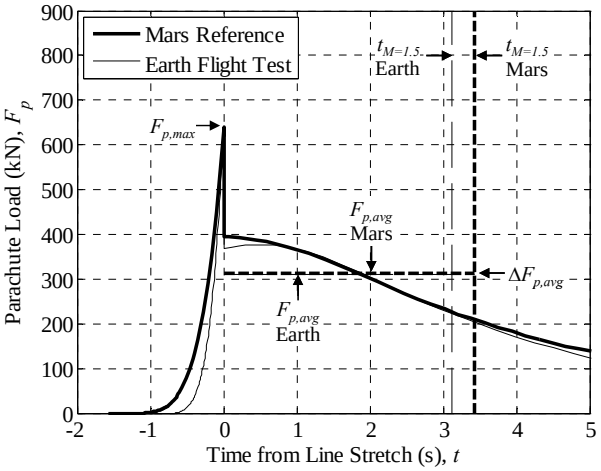

(b) Apparent mass model.

Fig. 4. Parachute load curves for γ_{Mars} = -30 deg.

5.3. Acceptable Range of Test Vehicle Masses

Given the results in Fig. 4, it appears that acceptable flight conditions (defined as within ±10% response difference from the reference) can be obtained for multiple test vehicle masses by flying a different trajectory. If this is true, then the test vehicle does not necessarily have to be ballasted to a specific mass in order to achieve the goals of the test flight – a change in trajectory will accomplish the same ends. To investigate this, initial flight path angles and altitudes are optimized for a range of test vehicle masses to determine their affect on the flight test responses. The resulting optimal combinations of flight path angle and test vehicle mass are shown in Fig. 5. Although not shown, optimal altitudes varied from 40 km for the lightest vehicle to 38 km for the heaviest.

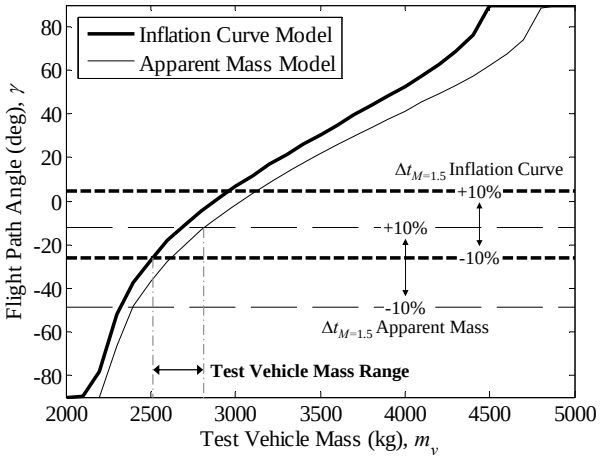

Fig. 5. Acceptable test vehicle mass range for γ_{Mars} = -30 deg.

The solid curves in the plot show the optimal parachute deployment flight path angle for a given test vehicle mass for each parachute force model. Along the solid lines, both $\Delta F_{p,max}$ and $\Delta F_{p,avg}$ are within ±10% of the reference Mars value. However, the $\Delta t_{M=1.5}$ value exceeds ±10% of the Mars reference value outside of the horizontal dotted lines shown in Fig. 5. Test vehicle mass is bounded on the low end by the $\Delta t_{M=1.5}$ constraint on the inflation curve optimization and bounded on the high end by the apparent mass optimization. Results show that a test vehicle ranging between about 2,500-2,700 kg will enable good responses during a flight test.

5.4. Sensitivity to Non-Optimal Flight Test Conditions

Because of uncertainties in the test environment, it may not be possible to fly an optimal trajectory. In order to assess the impact of a non-optimal flight test on the system responses, a design of experiments was performed over a range of flight path angles and altitudes for a fixed test vehicle mass. Contours representing the flight test design space are shown in Fig. 6.

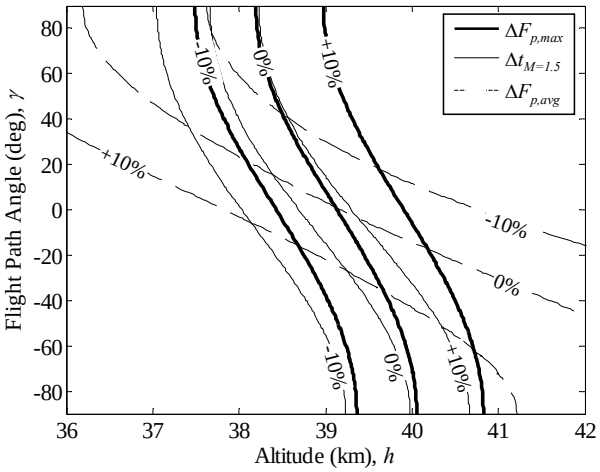

(a) Inflation curve model

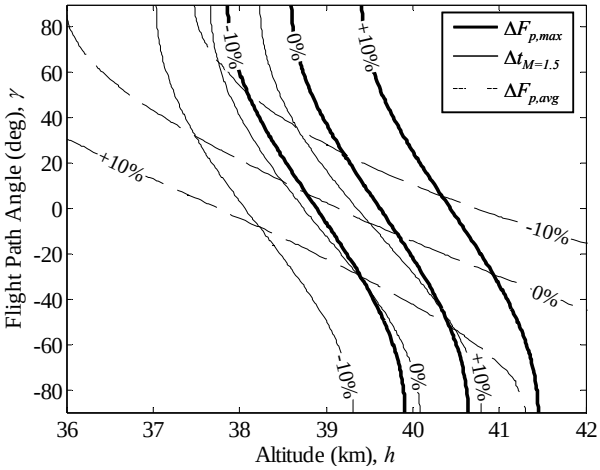

(b) Apparent mass model

Fig. 6. Earth flight test design space for m_v = 2900 kg and γ_{Mars} = -30 deg.

The thick solid contours are lines of $\Delta F_{p,max}$, thin solid contours are lines of $\Delta t_{M=1.5}$, and thin dashed contours are lines of $\Delta F_{p,avg}$. These contours illustrate three important parameters about the flight test design space. First, it is not possible to simultaneously achieve a match for both $\Delta F_{p,max}$ and $\Delta t_{M=1.5}$ – the 0% contour lines for the responses do not intersect. Second, the -10% constraint on $\Delta t_{M=1.5}$ is an active constraint for the apparent mass model optimization, causing the more negative flight path angles. This explains why the optimizer generated different results for the apparent mass case. Third, over a 10% change in the peak load will occur for a given flight path angle if the altitude is one kilometer higher or lower than the optimal altitude. This means that a 2.5% error (1 km error given a 40 km optimal altitude) in altitude will result in over a 10% error in peak load.

If a small error in altitude can elicit a large change in peak load, how difficult is it to obtain the optimal altitude? In other words, is how difficult is it to obtain a certain flight condition? Table 5 compares the conditions anticipated prior to the BLDT AV-4 test flight and the conditions actually witnessed by the flight test vehicle.

Table 5. Comparison of expected and actual flight conditions at AV-4 mortar fire [4].

	Expected	Flight	Difference
Mach Number	2.178	2.126	2.4%
Dyn Pressure (Pa)	519	522	0.57%
Velocity (m/s)	708.4	698.0	1.5%
Altitude (km)	43.78	44.86	2.4%

Table 5 illustrates that, given the proper test setup, the simulated (or expected) flight conditions can be obtained fairly accurately. However, it also shows that a 2.5% error in altitude is not a rare occurrence, potentially meaning greater than expected loads on the parachute.

6. CONCLUDING REMARKS

6.1. Conclusions

Several analyses were performed to determine the optimal flight test conditions to replicate the parachute loading environment that would be experienced at Mars. These analyses were performed assuming a relatively heavy Mars entry mass (4,000 kg) and the use of a large diameter (30 m) DGB parachute, deployed at high supersonic speed (Mach 3). Two opening loads models, an empirical inflation curve model and a more physically meaningful apparent mass model were used to optimize trajectories. Although it initially appeared that the two models were generating substantially different optimal conditions, it was shown that the two models actually generate similar responses. It was also shown that there is a range of test vehicle masses which can provide acceptable flight test results given optimal initial flight conditions.

6.2. Acknowledgements

The author would like to thank Dr. Juan Cruz for his guidance regarding this research as well as his editorial comments.

7. REFERENCES

1. Cruz, J.R., Kandis, M., Witkowski, A., “Opening Loads Analyses for Various Disk-Gap-Band Parachutes,” AIAA 2003-2131, *17th AIAA Aerodynamic Decelerator Systems Technology Conference and Seminar*, Monterey, California, May 2003.

2. Greene, G.C., “Opening Distance of a Parachute,” *Journal of Spacecraft and Rockets*, Vol. 7, No. 1, Jan 1970.

3. Wolf, D. “A Simplified Dynamic Model of Parachute Inflation,” AIAA 73-450, *4th AIAA Aerodynamic Deceleration Systems Conference*, Palm Springs, California, May 1973.

4. Dickinson, D., Schlemmer, J., Hicks, F., Michel, F., and Moog, R.D., “Balloon Launched Decelerator Test Program Post-Flight Test Report, BLDT Vehicle AV-4,” NASA CR-112179, 1972.

5. Talay, T.A., “Parachute Deployment Parameter Identification Based on an Analytical Simulation of Viking BLDT AV-4,” NASA TN D-7678, 1974.

6. Braun, R.D. and Manning, R.M., “Mars Exploration Entry, Descent, and Landing Challenges,” *Journal of Spacecraft and Rockets*, Vol. 44, No. 2, pp. 310-323, 2007.